Molecular Neuroprotection Induced by Zinc-Dependent Expression of Hepatitis C–Derived Protein NS5A Targeting Kv2.1 Potassium Channels

Jason A. Justice, Daniel T. Manjooran, Chung-Yang Yeh, Karen A. Hartnett-Scott, Anthony J. Schulien, Gabrielle J. Kosobucki, Shalom Mammen, Michael J. Palladino, and Elias Aizenman

Departments of Neurobiology (J.A.J., C.-Y.Y., K.A.H.-S., A.J.S., G.J.K., S.M., E.A.) and Pharmacology and Chemical Biology (D.T.M., M.J.P.) and Pittsburgh Institute for Neurodegenerative Diseases (J.A.J., D.T.M., C.-Y.Y., K.A.H.-S., A.J.S., G.J.K., S.M., M.J.P., E.A.), University of Pittsburgh School of Medicine, Pittsburgh, Pennsylvania

Received July 26, 2018; accepted September 6, 2018

ABSTRACT

We present the design of an innovative molecular neuroprotective strategy and provide proof-of-concept for its implementation, relying on the injury-mediated activation of an ectopic gene construct. As oxidative injury leads to the intracellular liberation of zinc, we hypothesize that tapping onto the zinc-activated metal regulatory element (MRE) transcription factor 1 system to drive expression of the Kv2.1-targeted hepatitis C protein NS5A (hepatitis C nonstructural protein 5A) will provide neuroprotection by preventing cell death–enabling cellular potassium loss in rat cortical neurons in vitro. Indeed, using biochemical and morphologic assays, we demonstrate rapid expression of MRE-driven products in neurons. Further, we report that MRE-driven NS5A expression, induced by a slowly evolving excitotoxic stimulus, functionally blocks injurious, enhanced Kv2.1 potassium whole-cell currents and improves neuronal viability. We suggest this form of "on-demand" neuroprotection could provide the basis for a tenable therapeutic strategy to prevent neuronal cell death in neurodegeneration.

Introduction

There are currently no effective pharmacotherapeutic approaches available to halt or slow the progressive neuronal cell loss evident in neurodegenerative disorders. With this in mind, we provide in vitro proof-of-concept for a novel, molecular approach for neuroprotection. This strategy was designed on the basis of three critical underlying concepts that are closely associated with neurodegenerative signaling cascades. First is the widely reported presence of oxidative stress in the vast majority, if not all, of neurodegenerative disorders, a process linked to neuronal cell death (Cicero et al., 2017; Liu et al., 2017; Cobley et al., 2018). Importantly, oxidative signals leading to the demise of neurons will always, likely without exception, lead to the liberation of intracellular zinc from metal-binding proteins (Maret, 2008, 2012; McCord and Aizenman, 2014). Second, a large number of cell types undergoing oxidant-induced cell death, including neurons, must lose intracellular potassium (Hughes and Cidlowski,

1999; Montague et al., 1999; Yu et al., 2001; Yu, 2003; Shah and Aizenman, 2014). The loss of potassium provides a "permissive" intracellular environment required for completion of many protease- and nuclease-dependent cell death cascades (Hughes and Cidlowski, 1999). We have shown that in mammalian central nervous system neurons, the loss of potassium is mediated via a syntaxin-dependent membrane insertion of a large number of Kv2.1 potassium channels (Pal et al., 2003, 2006; Shah and Aizenman, 2014). Critically, preventing the insertion of Kv2.1 into the plasma membrane via a variety of strategies, including blocking the interaction of Kv2.1 with syntaxin, is highly neuroprotective in vitro and in vivo (McCord et al., 2014; Yeh et al., 2017). Third, when zinc is liberated from a metal-binding protein as a result of oxidative conditions, cells normally react by inducing the expression of more metal-handling proteins as a homeostatic adaptive response. This is achieved by the binding of the liberated zinc to the metal regulatory element (MRE)–binding transcription factor 1 (MTF-1) (Daniels et al., 2002). Zinc, and seemingly only zinc (Daniels et al., 2002; Carpenter and Palmer, 2017), binds specifically to MTF-1 to promote its nuclear translocation, resulting in rapid transcription of MRE-driven genes and producing key proteins, including metallothionein (MT) and the zinc transporter

ABBREVIATIONS: GFP, green fluorescent protein; HCV, hepatitis C virus; Kv, voltage-gated potassium channel; MHB, minimum essential medium with HEPES and bovine serum albumin; MRE, metal regulatory element; MT, metallothionein; MTF-1, metal regulatory element transcription factor 1; NMDA, N-methyl-D-aspartate; NS5A, hepatitis C nonstructural protein 5A; ROI, region of interest; TBOA, DL-threo-β-benzyloxyaspartic acid.

ZnT1 (Andrews, 2000; Smirnova et al., 2000; Hardyman et al., 2016). Here, we hypothesize that the zinc-activated MTF-1/*MRE* system could be harnessed and adapted to express neuroprotective Kv2.1-targeted proteins, activated by the injurious process itself. That is, neurons would be reprogrammed to express a neuroprotective molecule but only when critically injured during oxidative stress conditions.

To begin to translate this innovative idea into practice, we constructed an *MRE*-containing vector driving the expression of the hepatitis C virus (HCV) protein NS5A (nonstructural protein 5A; Fig. 1). This protein was first shown to inhibit hepatocyte cell death by suppressing Kv2.1 function and limiting potassium efflux, a process proposed to facilitate viral persistence in the liver (Mankouri et al., 2009). Our group later showed that NS5A inhibited the cell death–inducing rise in functional membrane insertion of Kv2.1 in neurons by preventing a key Src-mediated phosphorylation event necessary for the interaction of the channel with the exocytotic protein syntaxin (Redman et al., 2009; Norris et al., 2012; He et al., 2015). In the present study, we demonstrate rapid expression of *MRE*-driven constructs in neurons following intracellular zinc liberation and, more importantly, *MRE*-NS5A–mediated suppression of cell death–facilitating potassium currents and neuroprotection following excitotoxic injury.

Materials and Methods

Cortical Neuronal Cell Culture Preparation. The Institutional Animal Care and Use Committee of the University of Pittsburgh School of Medicine approved the animal protocol described in this study, which was performed in accordance with the Guide for the Care and Use of Laboratory Animals as adopted and promulgated by the U.S. National Institutes of Health. Cortical neuronal cultures were prepared from embryonic day 16 to 17 rats of either sex as described previously (Hartnett et al., 1997; McCord et al., 2014). Pregnant donor rats (Charles River Laboratories, Wilmington, MA) were euthanized by regulated CO_2 inhalation, an American Veterinary Medical Association–approved protocol (Leary et al., 2013). Embryonic cortices were dissociated with trypsin and plated at 670,000 cells per well on 12-mm poly-L-lysine–coated coverslips in six-well plates (35-mm wells) as previously described (Hartnett et al.,
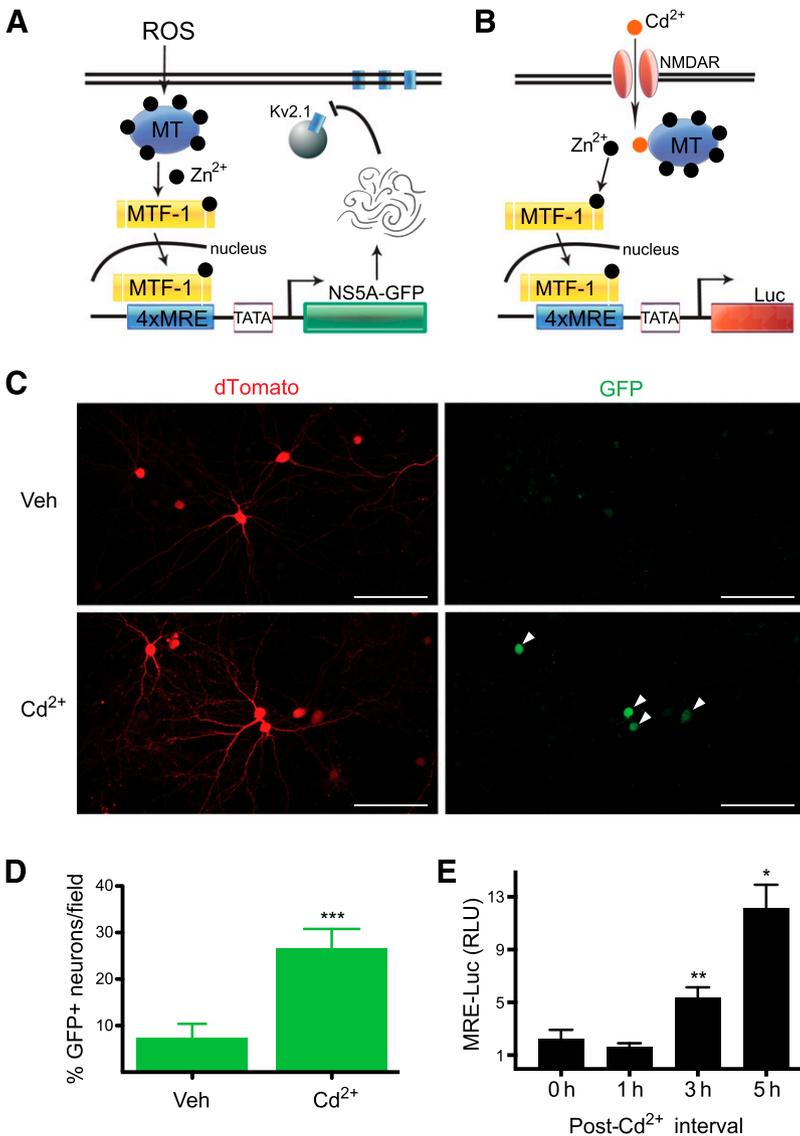
Fig. 1. Rapid neuronal expression of *MRE*-driven products. (A) Model for overall scheme presented here. Oxidative injury induces liberation of zinc from MT. The liberated zinc, in turn, activates MTF-1/*MRE*–driven expression of the Kv2.1-targeted protective molecule NS5A-GFP to prevent an apoptogenic increase in Kv2.1-mediated K$^+$ currents. (B) Rapid activation of *MRE*-driven expression initiated by influx of Cd^{2+} (20 μM, in the presence of 50 μM NMDA and 10 μM glycine for 10 minutes), which leads to displacement of zinc from MT and activation of the MTF-1/*MRE* system, driving the expression of firefly luciferase or NS5A-GFP in cortical neurons previously transfected with either *pLuc-MCS/4MREa* or *p4MRE-NS5A-GFP*. (C) Confocal images of cortical neurons cotransfected with *pCMV-dTomato* and *p4MRE-NS5A-GFP* were treated with either vehicle (Veh) or 20 μM CdCl$_2$ (in the presence of 50 μM NMDA and 10 μM glycine for 10 minutes). (Top panels) Images reflect weak, basal expression of GFP 5 hours following exposure to vehicle treatment. (Bottom panels) Images show four GFP-positive neurons in the field 5 hours following Cd^{2+}/NMDA/glycine exposure, demonstrating robust expression of NS5A-GFP. Arrows indicate neurons classified as GFP-positive by procedures described in the *Materials and Methods* section. All images were obtained with identical laser excitation power and image-acquisition settings. Scale bar, 100 μm. (D) Results show the mean percentage of GFP-positive neurons, as a proportion of all neurons visualized via dTomato fluorescence, per image field (403 mm^2) for each treatment. Values represent a total of three independent transfections, 10–13 visualized fields per condition (***$P < 0.001$; unpaired *t* test). (E) Quantification of *MRE*-driven luciferase expression in neurons following Cd^{2+} stimulation as described earlier. Cells were cotransfected with *pLuc-MCS/4MREa* and the constitutively expressed construct *pRL-TK* (*Renilla* luciferase). *MRE*-driven firefly luciferase units [relative light units (RLU)] were normalized to *Renilla* expression and are presented as a function of the post-Cd^{2+} exposure interval period. A one-way analysis of variance ($P = 0.003$) with post hoc Dunnett's multiple comparisons to the 0-hour time point revealed a significant increase in luciferase expression at the 3-hour (**$P < 0.01$) and 5-hour (*$P < 0.05$) time points. Results represent the mean ± S.E.M. of three independent experiments, each performed in quadruplicate. NMDAR, NMDA receptor; ROS, reactive oxygen species.

1997). Non-neuronal cell proliferation was inhibited with 1–2 μM cytosine arabinoside at 14 days in vitro. Cultures were used for all experimental protocols at 18–25 days in vitro. At this stage, the cultures contain approximately 20% neurons and 80% glia, most of which are astrocytes (Rosenberg and Aizenman, 1989).

Plasmids Used. The *MRE*–firefly luciferase construct (*pLuc-MCS/4MREa*) was a gift from D. Giedroc (Indiana University, Bloomington, IN). A vector expressing an NS5A-GFP fusion protein (*pNS5A-GFP*) was a gift from M. Harris (University of Leeds, Leeds, UK). These two vectors were used to generate an *MRE*-driven NS5A-GFP plasmid. In brief, the luciferase gene was excised from *pLuc-MCS/4MREa* by XbaI restriction digest. In its place, an ex-Taq polymerase polymerase chain reaction–amplified NS5A-GFP flanked with XbaI sites was inserted to create *p4MRE-NS5A-GFP*. The sequence of this construct was verified. The constitutively expressed firefly luciferase vector *pUHC13-3* was kindly provided by H. Bujard (Heidelberg, Germany). The tomato-expressing plasmid *pCMV-dTomato* was a gift from Z. Wills (University of Pittsburgh, Pittsburgh, PA). The empty vector plasmid *pCDNA3* was a gift from E. Levitan (University of Pittsburgh). Plasmids *pRL-TK* (*Renilla* firefly; Promega, Madison, WI) and *pBK* (empty vector; Stratagene, San Diego, CA) were purchased from commercial vendors. Table 1 summarizes the various plasmids used in these studies and their specific uses.

Transfection and Experimental Procedures. We took advantage of the fact that plasmids cotransfected together in neuronal cultures have a high probability (~90%) of being expressed together in any given cell (Santos and Aizenman, 2002). Cells were transfected in 1 ml of Dulbecco's minimum essential medium containing 2% HyClone (Thermo Fisher, Waltham, MA) calf serum with 2 μl of Lipofectamine 2000 (Invitrogen, Carlsbad, CA), 100 μl of Optimem (Gibco, Waltham, MA), and 1.5 μg of DNA per 15.5-mm well. For *MRE*-driven luciferase time-course experiments, cultures were transfected with 1 μg of *pLuc-MCS/4MREa*, 0.1 μg of empty vector *pBK*, and 0.4 μg of *Renilla* luciferase–expressing plasmid *pRL-TK* per 35-mm well. Twenty-four hours following transfection, the cultures were exposed for 10 minutes to 20 μM CdCl$_2$, 50 μM N-methyl-D-aspartate (NMDA), and 10 μM glycine in phenol red–free minimum essential medium supplemented with 25 mM HEPES and 0.01% bovine serum albumin (MHB) at 37°C and 5% CO$_2$. Following exposure, the coverslip was removed to a fresh well containing MHB and returned to the incubator. Firefly and *Renilla* luciferase signals were measured using the Dual Glo Luciferase Assay System (Promega) at 0, 1, 3, and 5 hours post-treatment. Results are expressed as a ratio of firefly to *Renilla* luciferase signal as described previously (Hara and Aizenman, 2004). For cell viability (luciferase) experiments, cultures were transfected with 0.375 μg of *pUHC13-3*, 0.75 μg of *p4MRE-NS5A-GFP*, and 0.375 μg of *pCDNA3* empty vector. The transfection mixture for control cultures contained additional empty vector in place of NS5A-expressing plasmid. Twenty-four hours after transfection, cultures were exposed continuously to 60 μM DL-*threo*-β-benzyloxyaspartic acid (TBOA; Tocris Bioscience, Bristol, UK), a broad-spectrum glutamate uptake inhibitor (Shimamoto et al., 1998). Firefly luciferase signal, as an index

of cell viability (Boeckman and Aizenman, 1996; Rameau et al., 2000; Aras et al., 2008), was measured at 24 hours using the Steadylite Plus Reporter Gene Assay System (PerkinElmer, Waltham, MA). This assay relies on the expression of luciferase by live neurons and closely correlates with the number of viable cells as described in detail and validated in a previously published methods paper (Aras et al., 2008).

For confocal microscopy and electrophysiological measurements, cultures were transfected with 0.75 μg of *p4MRE-NS5A-GFP*, 0.03 μg of *pCMV-dTomato*, and 0.72 μg of *pCDNA3* empty vector. The transfection mixture for control cultures contained additional empty vector in place of NS5A-expressing plasmid. For visualization of NS5A-GFP expression or cellular integrity, cells were treated at 24 hours post-transfection with vehicle or either the Cd^{2+}/NMDA/glycine mixture or TBOA as described earlier. Images were obtained with a Nikon A1+ confocal microscope using a 20× objective (Nikon Instruments, Melville, NY). Five to 10 optical sections (0.5 μm) were acquired to generate a maximum-intensity projection image. The injurious stimulus for electrophysiological experiments was a 2-hour exposure to 60 μM TBOA at 37°C and 5% CO$_2$. The solution was then slowly removed and cultures were carefully but thoroughly rinsed with MHB. Cells were then incubated for 2–4 hours (37°C) in MHB until electrophysiological measurements were conducted. The brief TBOA exposure was necessary to maintain cell integrity during the electrophysiological studies.

Quantification of NS5A-GFP–Positive Neurons Following Cd^{2+} Exposure. To analyze differences in GFP (488 nm) expression in *p4MRE-NS5A-GFP*–transfected neurons treated with vehicle or Cd^{2+}/NMDA/glycine, neurons (round soma, presence of dendrites) were first identified by visualization under dTomato red filter (561 nm). Regions of interest (ROIs) that represent neuronal somas were selected in Nikon NIS-Elements Advanced Research software utilizing the autoselect-ROI feature to consistently identify cell bodies in each imaging field. Background fluorescence was then subtracted from each image. From these refined ROIs, automated measurements of mean GFP intensity were obtained and imported into Excel (Microsoft, Redmond, WA) for further analysis. Vehicle-treated neurons (unexposed to Cd^{2+}/NMDA/glycine) were used to determine a standardized mean GFP intensity threshold for analysis. From these images, a GFP intensity of 166.7 relative fluorescent units (mean ± 1 S.D.) was set as the threshold for identifying a GFP-positive neuron in either the vehicle or Cd^{2+}/NMDA/glycine-treated group. These values were used to obtain a mean percentage of GFP-positive neurons per treatment, expressed as a function of all dTomato-positive neurons in each field. The final data points were inputted into GraphPad Prism (GraphPad Software, San Diego, CA) for statistical analysis. An unpaired, two-tailed *t* test was performed to analyze differences in each sample mean.

Dendritic Bleb Analysis. Glass coverslips containing neuronal cell cultures were placed in a recording chamber containing MHB. Live images were obtained via a Nikon A1R microscope at 20× magnification 48 hours after transfection and 24 hours after 60 μM TBOA treatment. Four field images were taken randomly from each

TABLE 1
Plasmids used in this study

Plasmid	Expressed Protein	Experimental Use	Relevant Figures
p4MRE-NS5A-GFP	MRE-driven NS5A-GFP fusion protein	MRE-driven NS5A-GFP time course; live confocal imaging; electrophysiology, cell viability assays	Figs. 1, C and D, 2, and 3
pLuc-MCS/4MREa	MRE-driven firefly luciferase	MRE-driven luciferase time course	Fig. 1E
pCMV-dTomato	dTomato red fluorescent protein	Live confocal imaging; neuronal visualization; dendritic bleb quantification	Figs. 1, C and D, 2A, and 3, C and D
pUHC13-3	Constitutively expressed firefly luciferase	Cell viability assays	Fig. 3, A and B
pRL-TK	Constitutively expressed *Renilla* luciferase	Cell viability assays	Fig. 1E
pBK; pCDNA3; pRGB4	Empty vectors	Experimental controls	All

coverslip. Z-stack series images were obtained with 2.325-μm step intervals and ranged from 12 to 24 steps per image. Maximum-intensity projections were generated from each Z-stack. The object count feature on the Nikon NIS-Elements Advanced Research software was used to assess quantitatively the number of blebs per field (Li et al., 2016). Although not all blebs present in a field belonged to one cell, the size of the field was always held constant across groups. The object count parameters were as follows: smooth, 1×; clean, 3×; separate, 1×; area, 0–30 μm^2; circularity, 0.5–1.0; mean intensity, 400–4095. Every experiment yielded an average number of bleb counts/field (403 mm^2) for each coverslip. All images during a particular experiment were gathered on the same day (e.g., NS5A-TBOA, NS5A-vehicle, vector-TBOA, vector-vehicle). Each transfection and subsequent imaging was repeated in three independent experiments, with $n = 24$ image fields obtained per treatment group. Four image fields for a given coverslip were averaged to obtain a value of $n = 6$ fields for each group. These data were used to obtain the sample mean for each treatment. For analysis of each treatment, the vector-vehicle group was used as a background signal, as there was no apparent blebbing in these groups. These values, likely reflecting counts of unusually large spines that may have been incorrectly counted as blebs, or other artifacts, were subtracted from the experimental group values.

Electrophysiological Recordings. Whole-cell voltage-clamp currents from rat cortical neurons were measured with an Axopatch 200B amplifier and pClamp software (Molecular Devices, San Jose, CA) using 3- to 5-MΩ electrodes and a 10-kHz low-pass filter (Justice et al., 2017). The extracellular solution contained 2 mM MgCl$_2$, 2.5 mM KCl, 115 mM NaCl, 10 mM HEPES, 10 mM D-glucose, 1 mM CaCl$_2$, and 0.25 μM tetrodotoxin, pH 7.2. The electrode solution contained 100 mM K-gluconate, 1 mM MgCl$_2$, 10 mM KCl, 1 mM CaCl$_2$, 2.2 mM MgCl$_2$·ATP, 0.33 mM GTP, 11 mM EGTA, and 10 mM HEPES, pH 7.2. Series resistance was compensated (~80%) in all cases. Despite the extensive dendritic arbors our neurons displayed, potential space-clamp problems were mitigated by the fact that Kv2.1 channels are restricted to the soma and very proximal processes (Maletic-Savatic et al., 1995). K$^+$ currents were evoked with a series of 200-ms voltage steps from a holding potential of −80 to +80 mV in 10-mV increments. A single 30-ms prepulse to +10 mV was used before depolarization to inactivate A-type K$^+$ currents. Mean steady-state delayed rectifier currents were measured relative to baseline at 180–190 ms after the initiation of each voltage step. Current amplitudes were normalized to cell capacitance values to generate the current density values presented in this study.

Data Presentation and Statistical Analysis. All data are expressed as the mean ± S.E.M., and statistical analyses were performed using GraphPad Prism software. The specific statistical analysis used and number of repetitions are specified for each figure and include pairwise comparisons, as well as analyses of variance with post hoc pairwise comparisons, appropriately corrected for multiple comparisons. Spreadsheets containing all raw data are available upon request from the corresponding author (E.A.).

Results

Rapid Expression of MRE-Driven Gene Products. The basic scheme behind the design of the novel neuroprotective strategy described in this study is depicted in Fig. 1A. Reactive oxygen species, or other pro-oxidants such as dithiols (Maret and Vallee, 1998; Aizenman et al., 2000), as well as reactive nitrogen species (St Croix et al., 2002; Zhang et al., 2004; Knoch et al., 2008) trigger the liberation of Zn^{2+} from metal-binding proteins, such as MT. Indeed, given its very negative ($< −365$ mV) redox potential, MT is well poised to serve as a primary cellular Zn^{2+} donor despite its relatively high affinity (K$_d$ = 1 × 10^{-14} M at neutral pH) for the metal

(Maret and Vallee, 1998). The liberated Zn^{2+}, in turn, binds to and promotes translocation of MTF-1 to the nucleus, inducing the activation of *MRE*-driven expression of the ectopic NS5A-GFP fusion protein (hereafter referred to as "NS5A"). Injured neurons, destined to die, begin the process of exocytotic insertion of Kv2.1 channels in the plasma membrane to facilitate cytosolic K$^+$ efflux within 3 hours following injury stimulus (McLaughlin et al., 2001; Pal et al., 2003). Cells expressing NS5A, however, are prevented from enacting this step and are given the opportunity to recover from the injurious insult, thereby surviving.

We previously reported that the enhanced K$^+$ currents observed in dying neurons begin to appear relatively slowly at approximately 3 hours following an acute, brief, lethal oxidative stimulus (McLaughlin et al., 2001). This delay in the current surge allows for a relatively comfortable temporal window for the expression of neuroprotective *MRE*-driven products. To confirm this, we exposed neurons previously transfected with either *p4MRE-NS5A-GFP* or *pLuc-MCS/4MREa* to a brief Cd^{2+} stimulus. Cd^{2+} is known to permeate through NMDA ionotropic glutamate receptor channels (Usai et al., 1999) and readily displace Zn^{2+} from MT due to its much-higher affinity for the metalloprotein (Waalkes et al., 1984) (Fig. 1B). The use of a nontoxic Cd^{2+} stimulus allowed us to measure the time course of *MRE*-driven expression induced by a defined temporal event without the complication of inducing neurotoxicity. Within 3–5 hours following a brief exposure to 20 μM Cd^{2+} (in the presence of 50 μM NMDA and 10 μM glycine, coagonists at the NMDA receptor), we observed relative robust expression of NS5A (GFP fluorescence) in significantly more transfected neurons when compared with vehicle-exposed cells (Fig. 1, C and D). This result suggests relatively small background activity of the ectopic gene but relatively rapid translation of the *MRE*-driven protein upon Zn^{2+} liberation. To accurately quantify the time course of this effect, we used the *MRE*-driven, luciferase-expressing plasmid in a separate set of cultures (Hara and Aizenman, 2004). Following a similar, brief exposure to Cd^{2+} in the presence of NMDA and glycine, we measured luciferase expression at several time points, noting pronounced, significant increases in signal within 3–5 hours following Cd^{2+} exposure (Fig. 1D). At the 3-hour time point, luciferase expression was close to 5 times the baseline signal observed immediately or 1 hour following the Cd^{2+} exposure, whereas at 5 hours, the signal additionally doubled to levels approximately 10 times what was observed at baseline (Fig. 1D). Altogether, these results strongly suggest that *MRE*-driven proteins can be expressed at a sufficiently rapid rate to likely prevent the completion of injurious cellular cascade allowed by a Kv2.1-dependent K$^+$ current surge.

MRE-Driven Expression of NS5A Prevents K$^+$ Current Surge. To investigate whether *MRE*-driven expression of NS5A is effective in preventing the enhancement of cell death–enabling K$^+$ currents, we performed whole-cell patch-clamp recordings in *p4MRE-NS5A-GFP*–transfected cortical neurons previously exposed to the glutamate uptake inhibitor TBOA (60 μM). We chose glutamate uptake inhibition as the injurious stimulus as this method generates a relatively "slow" (a few hours) excitotoxic injury that induces a Kv2.1-mediated cell death process (Yeh et al., 2017). This is likely because glutamate uptake inhibition preferentially damages

A

TBOA (5hr)

Tomato   NS5A-GFP

B

C

D
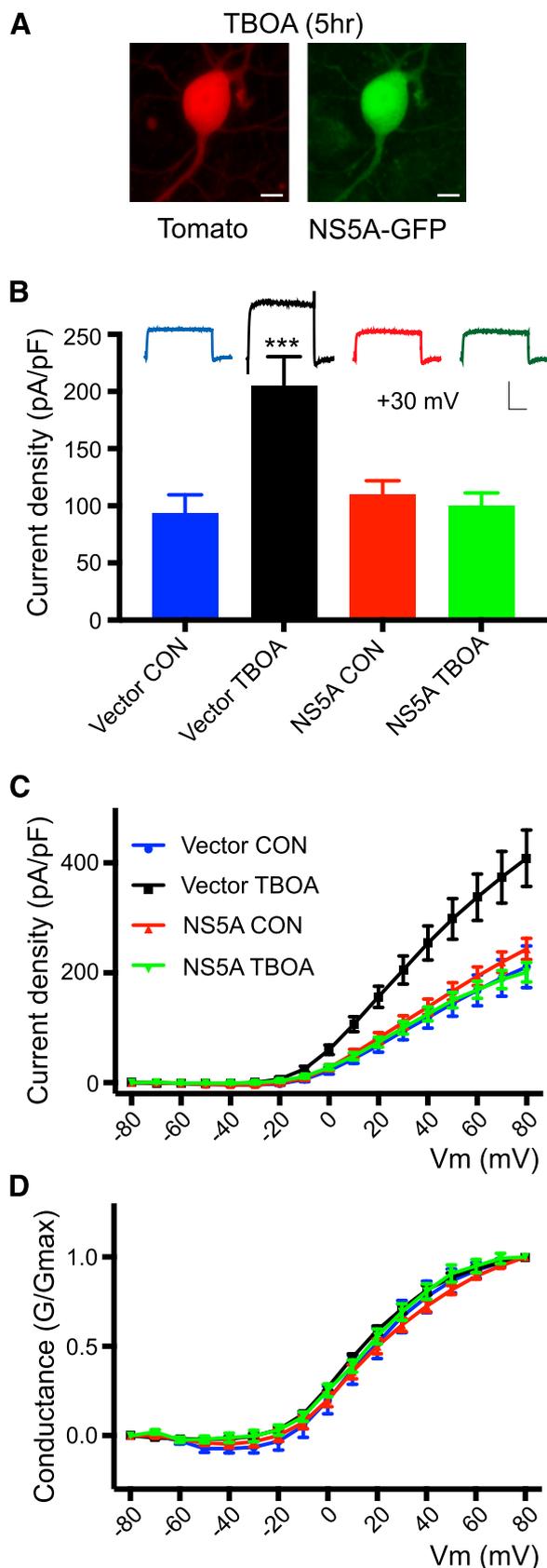
Fig. 2. *MRE*-driven NS5A expression suppresses enhanced K$^+$ currents following excitotoxic injury. (A) Fluorescent image of a cortical neuron expressing dTomato and NS5A-GFP 4 hours following a 2-hour 60 μM TBOA treatment (and subsequent 2-hour wash). Scale bar, 20 μm. (B) Mean K$^+$ current density (pA/pF) profiles (top) and mean $\pm$ S.E.M values

neurons via NMDA receptor activation (Blitzblau et al., 1996), an established source of reactive oxygen species (Blitzblau et al., 1996), intracellular zinc liberation (Dineley et al., 2008; Granzotto and Sensi, 2015), and Kv2.1-mediated excitotoxicity (Yao et al., 2009). We used a 2-hour exposure to TBOA and visually confirmed expression of NS5A as a GFP fluorescent signal 4 hours after the initiation of the treatment (Fig. 2A). Recordings were then obtained from cells transfected with the *MRE*-driven NS5A construct or with empty vector at approximately 4–6 hours after the initiation of a 2-hour TBOA exposure (see *Transfection and Experimental Procedures*). We observed a dramatic enhancement in K$^+$ current densities in vector-expressing cells exposed to TBOA when compared with vehicle (Fig. 2, B and C). Indeed, measurements at the $+$30-mV voltage step demonstrated a significant doubling of current density in the injured cells (Fig. 2B). Notably, the TBOA-mediated K$^+$ current surge did not occur in cells transfected with the *MRE*-driven NS5A construct, suggesting that Zn^{2+}-induced expression of the viral protein was sufficient to prevent the cell death enhancement of Kv2.1-mediated currents (Fig. 2, B and C). Importantly, current densities in *p4MRE-NS5A-GFP*–transfected cells, regardless of the presence or absence of TBOA treatment, were not different from empty vector–expressing cells under control conditions (Fig. 2, B and C), indicating that the rapid expression of NS5A in injured cells was sufficient to hinder the development of enhanced, cell death–facilitating K$^+$ currents without affecting normal current levels. Finally, we observed very similar channel voltage activation profiles in all of the experimental groups (Fig. 2D), suggesting that 1) the observed changes in Kv2.1 function following TBOA exposure are distinct from other forms of channel modulation not directly related to cell death (Mohapatra et al., 2007); and 2) NS5A expression, as reported previously (Norris et al., 2012; Clemens et al., 2015), does not substantially affect normal channel function. The half-maximal activation voltages for all experimental groups were as follows: vector/vehicle, 21.09 $\pm$ 2.79 mV (n = 12); vector/TBOA, 14.58 $\pm$ 1.26 mV (n = 12); NS5A/vehicle, 20.14 $\pm$ 2.57 mV (n = 12); and NS5A/TBOA 18.78 $\pm$ 2.80 mV (n = 10).

MRE-Driven Expression of NS5A Is Neuroprotective. The observed inhibition of K$^+$ current surges in injured neurons by *MRE*-driven NS5A expression suggests that this same process would render neurons resistant to a lethal injury and improve viability. To test this, we exposed vector or *p4MRE-NS5A-GFP*–transfected neurons to an overnight

(bottom) at a -80- to $+30$-mV voltage step for neurons exposed to either vehicle or 60 μM TBOA as detailed earlier. Cells were either transfected with empty vector or *p4MRE-NS5A-GFP* (pA/pF). A one-way analysis of variance ($P < 0.0001$) with Sidak's post hoc comparisons between means revealed a significant increase in K$^+$ current density in empty vector–transfected cells treated with TBOA (n = 12) when compared with vehicle (n = 12; ***$P < 0.001$). In contrast, no differences were observed between treatment groups in *p4MRE-NS5A-GFP*–expressing cells. Scale bar, 100 pA/pF; 50 ms. (C) Full current density-voltage relationships for all groups denoted in (B); note the increase in current densities in TBOA-exposed, empty vector–transfected cells when compared with all other groups and the lack of change in overall profile in NS5A-expressing cells. (D) Normalized conductance (G/G$_{max}$)-voltage relationships for all experimental groups. Note the similar activation profiles for all cells. Half-maximal activation voltages (V$_{1/2}$) are detailed in the text. CON, control.

treatment with 60 μM TBOA. Viability was assessed via a luciferase expression assay that we previously characterized for transfected cells, where luciferase activity tightly correlates to the number of live neurons in the culture (Aras et al., 2008). Please note that the luciferase-expressing vector used in these studies is constitutively expressed and not *MRE*-driven (Table 1). Figure 3A shows the results from a single experiment with raw luciferase activity values (as relative light units). TBOA induced an approximately 50% decrease in viability in vector-expressing cells. In contrast, neurons previously transfected with the NS5A-expressing plasmid were able to better withstand this insult. Results are summarized for four independent experiments in Fig. 3B, with viability expressed as a percentage of control (TBOA/vehicle) for each transfection (vector or *p4MRE-NS5A-GFP*). Finally, we visualized this phenomenon in *pCMV-dTomato* cotransfected neurons (Fig. 3C). Vector-expressing cells exposed overnight to TBOA showed substantial dendritic blebbing not dissimilar from that produced by gain-of-function mutations of NMDA receptor subunits reported previously (Li et al., 2016; Ogden et al., 2017). In contrast, cells rescued by NS5A expression maintained their integrity in the presence of the excitotoxin. We quantified the extent of dendritic blebbing by an automated, unbiased procedure (Ogden et al., 2017) (described

in detail in the *Materials and Methods* section) and observed a significant decrease in blebs in neurons expressing *p4MRE-NS5A-GFP*, demonstrating, via an independent analysis, the neuroprotective actions of the *MRE*-driven expression of the viral protein. These exciting results strongly suggest that the MTF-1/*MRE* system can be adapted to express neuroprotective molecules, at least when directed to Kv2.1-facilitated forms of cell death.

Discussion

Although several mechanisms have been proposed to account for the demise of neurons in neurodegenerative disorders, the fact remains that we do not generally know how or when any given neuron or group of neurons will die in the course of a disease. This is a critical problem to solve, as designing optimal new therapies for neurodegenerative disorders would ideally target specific cell death cascade processes nearer to the moment they are activated during pathogenesis. Addressing this specific issue, we present an adaptation of two important signaling pathway components. These have been harnessed toward the design, construction, and implementation of a novel neuroprotective method that targets, when activated, an apparent requisite element in oxidant-induced cell death: the
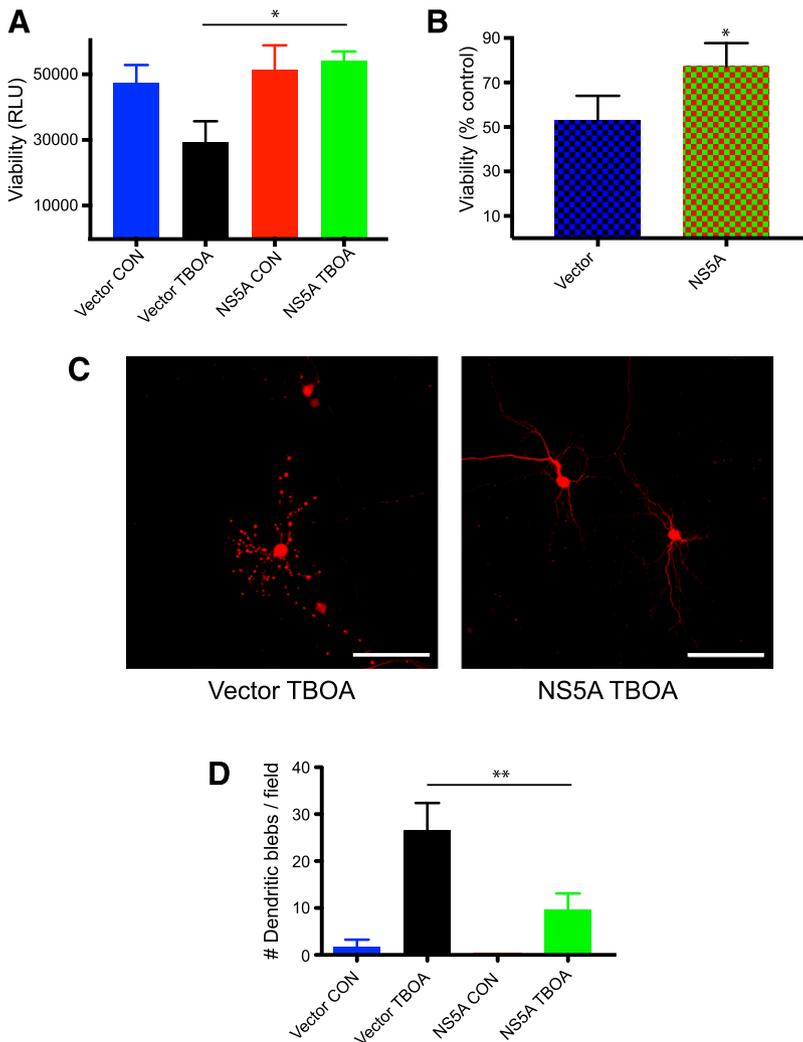
Fig. 3. *MRE*-driven NS5A is neuroprotective. (A) Results from a single experiment performed in quadruplicate denoting luciferase activity [in relative light units (RLU)] as an index of viability as described previously (Aras et al., 2008). Neurons transfected with *pUHC13-3* and with either empty vector or *p4MRE-NS5A-GFP* were exposed overnight to either vehicle or 60 μM TBOA. Luciferase assays revealed a significant decrease in viability in vector-expressing cells treated with TBOA, which was not observed in NS5A-expressing cells. Statistical analysis was performed by a one-way analysis of variance followed by Sidak's multiple comparisons tests (*$P <$ 0.05). (B) Pooled data for four independent experiments similar to that shown in (A), each performed in quadruplicate with viability expressed as a percentage of control (TBOA/vehicle for both vector and *MRE*-driven NS5A-expressing cells). A significant increase in viability was observed in *MRE*-driven NS5A-expressing cells when compared with vector-transfected neurons (*$P <$ 0.05, two-tailed *t* test). (C) Visualization of neuroprotective actions of MRE-driven NS5A expression. A separate set of cultures were cotransfected with *pCMV-dTomato* and imaged with a confocal microscope to capture neuronal integrity in NS5A-expressing neurons exposed to TBOA when compared with vector-expressing cells. Note the lack of neurite blebbing in NS5A-expressing cells when compared with vector-expressing cells. Scale bar, 100 μm. (D) Quantification of dendritic damage by TBOA exposure. Data represent the average number of dendritic swellings (blebs) per confocal imaging field (403 mm^2). Neurons were transfected with either empty vector or *p4MRE-NS5A-GFP* and subsequently exposed to either vehicle (MHB) or 60 μM TBOA for 24 hours in three independent experiments similar to (A). Please see the *Materials and Methods* section for a detailed description of procedures. A significant decrease in dendritic blebs was found in the NS5A-expressing group treated with TBOA compared with the vector-expressing group. Analyzed via one-way analysis of variance followed by Sidak's multiple comparisons test (**$P <$ 0.01). CON, XXX.

loss of intracellular K^+ (Shah and Aizenman, 2014). The first critical component of the neuroprotective strategy described here is the HCV protein NS5A, whereas the second one is the zinc-sensing MTF-1/MRE gene–expression system. Most importantly, however, is the fact that a number of studies support the notion that a major conduit for cellular K^+ loss in a variety of injured neuronal populations, including cortical, nigral, hippocampal, striatal, and cerebellar granule neurons, is the voltage-dependent, delayed-rectifier K^+ channel Kv2.1 (Pal et al., 2003; Redman et al., 2006; Dallas et al., 2011; Shepherd et al., 2012; Zhou et al., 2012; Yeh et al., 2017; Liu et al., 2018), a previously described target of NS5A (Mankouri et al., 2009; Norris et al., 2012). As a brief aside, although Kv2.1 has classically been connected with the activation of apoptotic programs (Yu, 2003), other studies have implicated Kv2.1 in oxidant-induced cell death processes not necessarily associated with classic apoptosis (Ito et al., 2017), including toxin-mediated dopaminergic cell death (Redman et al., 2006; Chao et al., 2018), suggesting a wider applicability of our proposed work. Also, cellular K^+ loss may enable neurodegenerative cascades associated with either histone deacetylase (D'Mello, 2009; Lin et al., 2017; Sixto-Lopez et al., 2018) or NLRP3 inflammasome activation (He et al., 2016; Zhou et al., 2016), although Kv2.1 has not yet been directly associated with these processes.

Investigating the mechanism of HCV persistence in the liver, Mankouri et al. (2009) discovered that hepatocytes also use Kv2.1 to undergo programmed cell death. This process, however, is halted in viral-infected cells, as HCV evolved a function within one of its 10 encoded proteins, namely, NS5A, to block the increase in Kv2.1 surface expression during the apoptotic program (Mankouri et al., 2009). Mankouri et al. (2009) proposed this as a mechanism for aiding HCV in establishing a chronic infection in an organ with relatively rapid cell turnover. As mentioned earlier, after obtaining an NS5A-expressing plasmid from the laboratory of M. Harris (University of Leeds), we showed it to be highly neuroprotective against oxidative injury in cortical neurons (Norris et al., 2012). Moreover, we demonstrated that, in neurons, NS5A worked by preventing a key Src phosphorylation step of Kv2.1, necessary for the channel's apoptotic insertion in the cell membrane (Redman et al., 2009; Norris et al., 2012; He et al., 2015). Critically, overexpression of NS5A in neurons had no substantial effect on their resting membrane potential, input resistance, threshold synaptic conductance, and firing frequency as a function of current (Norris et al., 2012). These observations encouraged us to use NS5A in an MRE-driven vector, essentially attempting to mimic part of a mechanism that evolved in a virus to prevent cell death, which, astonishingly, targeted Kv2.1. It is worth noting at this point that NS5A is also the site of action of ledipasvir, a principal component of a highly successful HCV antiviral drug (Pawlotsky, 2013). We found, however, that the presence of ledipasvir does not influence the activity of NS5A on the Kv2.1 channel, suggesting that other components of the viral protein are critical for K^+ channel inhibition (Clemens et al., 2015).

NS5A is an ~447–amino acid, multicomponent protein that also contains a zinc finger domain near its N terminus (He et al., 2006). Since zinc chelators can prevent K^+ current enhancement following oxidative injury (McLaughlin et al., 2001), it is conceivable that MRE-driven NS5A expression could also function as a chelator of this metal. However, several lines of evidence previously discounted the possibility

of this protein acting as a physiologic zinc buffer in our model. First, in the original description of the effects of NS5A on Kv2.1 in hepatocytes, Mankouri et al. (2009) showed that polyproline to alanine mutations near the C terminus did not inhibit the channel, with the zinc finger remaining intact. Second, some NS5A genotypes do not seem to inhibit Kv2.1 function, yet all genotypes contain a zinc finger domain (Norris et al., 2012). Third, inhibition of phosphorylation of NS5A by casein kinase II prevents the effects of the viral protein on Kv2.1. The casein kinase II phosphorylation site(s) is also very close to the C terminus, well away from the zinc finger domain. As such, the evidence strongly points to the inhibition of Src phosphorylation of Kv2.1 as a principal mechanism of NS5A-mediated neuroprotection (Norris et al., 2012).

Injury-triggered translation of cytoprotective proteins has been explored previously. Human heme oxygenase, driven by the hypoxia response element promoter, was successfully demonstrated to induce cardioprotection following ischemic injury (Pachori et al., 2004). Our results suggest that the four MRE tandem sequences in our vector are sufficient to rapidly trigger expression of gene products and, most importantly, generate a neuroprotective protein within the cells that has a specific target, namely, Kv2.1. We foresee translating this technique in the near future with neurotropic viral vectors, such as the blood-brain barrier–permeable AAV9 (Saraiva et al., 2016), to test the effectiveness of this strategy in in vivo models of chronic/progressive models of neurodegenerative disorders, including genetic animal models. The results presented here strongly suggest that a molecular form of "on-demand" neuroprotection may be a viable alternative or complementary strategy to combat neurodegeneration in humans in the years ahead.

Authorship Contributions

Participated in research design: Aizenman, Palladino, Justice, Manjooran, Yeh.

Conducted experiments: Justice, Manjooran, Hartnett-Scott, Schulien, Kosobucki, Mammen.

Performed data analysis: Justice, Aizenman.

Wrote or contributed to the writing of the manuscript: Justice, Aizenman.

References

Aizenman E, Stout AK, Hartnett KA, Dineley KE, McLaughlin B, and Reynolds IJ (2000) Induction of neuronal apoptosis by thiol oxidation: putative role of intracellular zinc release. *J Neurochem* 75:1878–1888.

Andrews GK (2000) Regulation of metallothionein gene expression by oxidative stress and metal ions. *Biochem Pharmacol* 59:95–104.

Aras MA, Hartnett KA, and Aizenman E (2008) Assessment of cell viability in primary neuronal cultures. *Curr Protoc Neurosci* 44:Unit 7.18.1–7.18.15.

Blitzblau R, Gupta S, Djali S, Robinson MB, and Rosenberg PA (1996) The glutamate transport inhibitor L-trans-pyrrolidine-2,4-dicarboxylate indirectly evokes NMDA receptor mediated neurotoxicity in rat cortical cultures. *Eur J Neurosci* 8:1840–1852.

Boeckman FA and Aizenman E (1996) Pharmacological properties of acquired excitotoxicity in Chinese hamster ovary cells transfected with N-methyl-D-aspartate receptor subunits. *J Pharmacol Exp Ther* 279:515–523.

Carpenter MC and Palmer AE (2017) Native and engineered sensors for Ca^{2+} and Zn^{2+}: lessons from calmodulin and MTF1. *Essays Biochem* 61:237–243.

Chao RY, Cheng CH, Wu SN, and Chen PC (2018) Defective trafficking of Kv2.1 channels in MPTP-induced nigrostriatal degeneration. *J Neurochem* 144:483–497.

Cicero CE, Mostile G, Vasta R, Rapisarda V, Signorelli SS, Ferrante M, Zappia M, and Nicoletti A (2017) Metals and neurodegenerative diseases. A systematic review. *Environ Res* 159:82–94.

Clemens K, Yeh CY, and Aizenman E (2015) Critical role of Casein kinase 2 in hepatitis C NS5A-mediated inhibition of Kv2.1 K(+) channel function. *Neurosci Lett* 609:48–52.

Cobley JN, Fiorello ML, and Bailey DM (2018) 13 reasons why the brain is susceptible to oxidative stress. *Redox Biol* 15:490–503.

Dallas ML, Boyle JP, Milligan CJ, Sayer R, Kerrigan TL, McKinstry C, Lu P, Mankouri J, Harris M, Scragg JL, et al. (2011) Carbon monoxide protects against oxidant-induced apoptosis via inhibition of Kv2.1. *FASEB J* 25:1519–1530.

Daniels PJ, Bittel D, Smirnova IV, Winge DR, and Andrews GK (2002) Mammalian metal response element-binding transcription factor-1 functions as a zinc sensor in yeast, but not as a sensor of cadmium or oxidative stress. *Nucleic Acids Res* 30:3130–3140.

Dineley KE, Devinney MJ, II, Zeak JA, Rintoul GL, and Reynolds IJ (2008) Glutamate mobilizes [Zn2+] through Ca2+ -dependent reactive oxygen species accumulation. *J Neurochem* 106:2184–2193.

D'Mello SR (2009) Histone deacetylases as targets for the treatment of human neurodegenerative diseases. *Drug News Perspect* 22:513–524.

Granzotto A and Sensi SL (2015) Intracellular zinc is a critical intermediate in the excitotoxic cascade. *Neurobiol Dis* 81:25–37.

Hara H and Aizenman E (2004) A molecular technique for detecting the liberation of intracellular zinc in cultured neurons. *J Neurosci Methods* 137:175–180.

Hardyman JE, Tyson J, Jackson KA, Aldridge C, Cockell SJ, Wakeling LA, Valentine RA, and Ford D (2016) Zinc sensing by metal-responsive transcription factor 1 (MTF1) controls metallothionein and ZnT1 expression to buffer the sensitivity of the transcriptome response to zinc. *Metallomics* 8:337–343.

Hartnett KA, Stout AK, Rajdev S, Rosenberg PA, Reynolds IJ, and Aizenman E (1997) NMDA receptor-mediated neurotoxicity: a paradoxical requirement for extracellular Mg2+ in Na+/Ca2+-free solutions in rat cortical neurons in vitro. *J Neurochem* 68:1836–1845.

He K, McCord MC, Hartnett KA, and Aizenman E (2015) Regulation of pro-apoptotic phosphorylation of Kv2.1 K+ channels. *PLoS One* 10:e0129498.

He Y, Hara H, and Núñez G (2016) Mechanism and regulation of NLRP3 inflammasome activation. *Trends Biochem Sci* 41:1012–1021.

He Y, Staschke KA, and Tan SL (2006) HCV NS5A: a multifunctional regulator of cellular pathways and virus replication, in *Hepatitis C Viruses: Genomes and Molecular Biology* (Tan SL ed), Horizon Bioscience, Norfolk, UK.

Hughes FM Jr and Cidlowski JA (1999) Potassium is a critical regulator of apoptotic enzymes in vitro and in vivo. *Adv Enzyme Regul* 39:157–171.

Ito K, Eguchi Y, Imagawa Y, Akai S, Mochizuki H, and Tsujimoto Y (2017) MPP+ induces necrostatin-1- and ferrostatin-1-sensitive necrotic death of neuronal SH-SY5Y cells. *Cell Death Discov* 3:17013.

Justice JA, Schulien AJ, He K, Hartnett KA, Aizenman E, and Shah NH (2017) Disruption of K$_V$2.1 somato-dendritic clusters prevents the apoptogenic increase of potassium currents. *Neuroscience* 354:158–167.

Knoch ME, Hartnett KA, Hara H, Kandler K, and Aizenman E (2008) Microglia induce neurotoxicity via intraneuronal Zn(2+) release and a K(+) current surge. *Glia* 56:89–96.

Leary S, Underwood W, Anthony R, Cartner S, Corey D, Grandin T, Greenacre CB, Gwaltney-Bran S, McCrackin MA, and Meyer R (2013) *AVMA Guidelines for the Euthanasia of Animals: 2013 Edition*, American Veterinary Medical Association, Schaumburg, IL.

Li D, Yuan H, Ortiz-Gonzalez XR, Marsh ED, Tian L, McCormick EM, Kosobucki GJ, Chen W, Schulien AJ, Chiavacci R, et al. (2016) GRIN2D recurrent de novo dominant mutation causes a severe epileptic encephalopathy treatable with NMDA receptor channel blockers. *Am J Hum Genet* 99:802–816.

Lin YH, Dong J, Tang Y, Ni HY, Zhang Y, Su P, Liang HY, Yao MC, Yuan HJ, Wang DL, et al. (2017) Opening a new time window for treatment of stroke by targeting HDAC2. *J Neurosci* 37:6712–6728.

Liu F, Zhang Y, Liang Z, Sun Q, Liu H, Zhao J, Xu J, Zheng J, Yun Y, Yu X, et al. (2018) Cleavage of potassium channel Kv2.1 by BACE2 reduces neuronal apoptosis. *Mol Psychiatry* 23:1542–1554.

Liu Z, Zhou T, Ziegler AC, Dimitrion P, and Zuo L (2017) Oxidative stress in neurodegenerative diseases: from molecular mechanisms to clinical applications. *Oxid Med Cell Longev* 2017:2525967.

Maletic-Savatic M, Lenn NJ, and Trimmer JS (1995) Differential spatiotemporal expression of K+ channel polypeptides in rat hippocampal neurons developing in situ and in vitro. *J Neurosci* 15:3840–3851.

Mankouri J, Dallas ML, Hughes ME, Griffin SD, Macdonald A, Peers C, and Harris M (2009) Suppression of a pro-apoptotic K+ channel as a mechanism for hepatitis C virus persistence. *Proc Natl Acad Sci USA* 106:15903–15908.

Maret W (2008) Metallothionein redox biology in the cytoprotective and cytotoxic functions of zinc. *Exp Gerontol* 43:363–369.

Maret W (2012) New perspectives of zinc coordination environments in proteins. *J Inorg Biochem* 111:110–116.

Maret W and Vallee BL (1998) Thiolate ligands in metallothionein confer redox activity on zinc clusters. *Proc Natl Acad Sci USA* 95:3478–3482.

McCord MC and Aizenman E (2014) The role of intracellular zinc release in aging, oxidative stress, and Alzheimer's disease. *Front Aging Neurosci* 6:77.

McCord MC, Kullmann PH, He K, Hartnett KA, Horn JP, Lotan I, and Aizenman E (2014) Syntaxin-binding domain of Kv2.1 is essential for the expression of apoptotic K+ currents. *J Physiol* 592:3511–3521.

McLaughlin B, Pal S, Tran MP, Parsons AA, Barone FC, Erhardt JA, and Aizenman E (2001) p38 activation is required upstream of potassium current enhancement and caspase cleavage in thiol oxidant-induced neuronal apoptosis. *J Neurosci* 21:3303–3311.

Mohapatra DP, Park KS, and Trimmer JS (2007) Dynamic regulation of the voltage-gated Kv2.1 potassium channel by multisite phosphorylation. *Biochem Soc Trans* 35:1064–1068.

Montague JW, Bortner CD, Hughes FM Jr, and Cidlowski JA (1999) A necessary role for reduced intracellular potassium during the DNA degradation phase of apoptosis. *Steroids* 64:563–569.

Norris CA, He K, Springer MG, Hartnett KA, Horn JP, and Aizenman E (2012) Regulation of neuronal proapoptotic potassium currents by the hepatitis C virus nonstructural protein 5A. *J Neurosci* 32:8865–8870.

Ogden KK, Chen W, Swanger SA, McDaniel MJ, Fan LZ, Hu C, Tankovic A, Kusumoto H, Kosobucki GJ, Schulien AJ, et al. (2017) Molecular mechanism of disease-associated mutations in the pre-M1 helix of NMDA receptors and potential rescue pharmacology. *PLoS Genet* 13:e1006536.

Pachori AS, Melo LG, Hart ML, Noiseux N, Zhang L, Morello F, Solomon SD, Stahl GL, Pratt RE, and Dzau VJ (2004) Hypoxia-regulated therapeutic gene as a preemptive treatment strategy against ischemia/reperfusion tissue injury. *Proc Natl Acad Sci USA* 101:12282–12287.

Pal S, Hartnett KA, Nerbonne JM, Levitan ES, and Aizenman E (2003) Mediation of neuronal apoptosis by Kv2.1-encoded potassium channels. *J Neurosci* 23:4798–4802.

Pal SK, Takimoto K, Aizenman E, and Levitan ES (2006) Apoptotic surface delivery of K+ channels. *Cell Death Differ* 13:661–667.

Pawlotsky JM (2013) NS5A inhibitors in the treatment of hepatitis C. *J Hepatol* 59:375–382.

Rameau GA, Akaneya Y, Chiu L, and Ziff EB (2000) Role of NMDA receptor functional domains in excitatory cell death. *Neuropharmacology* 39:2255–2266.

Redman PT, Hartnett KA, Aras MA, Levitan ES, and Aizenman E (2009) Regulation of apoptotic potassium currents by coordinated zinc-dependent signalling. *J Physiol* 587:4393–4404.

Redman PT, Jefferson BS, Ziegler CB, Mortensen OV, Torres GE, Levitan ES, and Aizenman E (2006) A vital role for voltage-dependent potassium channels in dopamine transporter-mediated 6-hydroxydopamine neurotoxicity. *Neuroscience* 143:1–6.

Rosenberg PA and Aizenman E (1989) Hundred-fold increase in neuronal vulnerability to glutamate toxicity in astrocyte-poor cultures of rat cerebral cortex. *Neurosci Lett* 103:162–168.

Santos S and Aizenman E (2002) Functional expression of muscle-type nicotinic acetylcholine receptors in rat forebrain neurons in vitro. *Methods Find Exp Clin Pharmacol* 24:63–66.

Saraiva J, Nobre RJ, and Pereira de Almeida L (2016) Gene therapy for the CNS using AAVs: the impact of systemic delivery by AAV9. *J Control Release* 241:94–109.

Shah NH and Aizenman E (2014) Voltage-gated potassium channels at the crossroads of neuronal function, ischemic tolerance, and neurodegeneration. *Transl Stroke Res* 5:38–58.

Shepherd AJ, Loo L, Gupte RP, Mickle AD, and Mohapatra DP (2012) Distinct modifications in Kv2.1 channel via chemokine receptor CXCR4 regulate neuronal survival-death dynamics. *J Neurosci* 32:17725–17739.

Shimamoto K, Lebrun B, Yasuda-Kamatani Y, Sakaitani M, Shigeri Y, Yumoto N, and Nakajima T (1998) DL-threo-beta-benzyloxyaspartate, a potent blocker of excitatory amino acid transporters. *Mol Pharmacol* 53:195–201.

Sixto-López Y, Bello M, and Correa-Basurto J (2018) Insights into structural features of HDAC1 and its selectivity inhibition elucidated by Molecular dynamic simulation and Molecular Docking. *J Biomol Struct Dyn* 6:1–27.

Smirnova IV, Bittel DC, Ravindra R, Jiang H, and Andrews GK (2000) Zinc and cadmium can promote rapid nuclear translocation of metal response element-binding transcription factor-1. *J Biol Chem* 275:9377–9384.

St Croix CM, Wasserloos KJ, Dineley KE, Reynolds IJ, Levitan ES, and Pitt BR (2002) Nitric oxide-induced changes in intracellular zinc homeostasis are mediated by metallothionein/thionein. *Am J Physiol Lung Cell Mol Physiol* 282:L185–L192.

Usai C, Barberis A, Moccagatta L, and Marchetti C (1999) Pathways of cadmium influx in mammalian neurons. *J Neurochem* 72:2154–2161.

Waalkes MP, Harvey MJ, and Klaassen CD (1984) Relative in vitro affinity of hepatic metallothionein for metals. *Toxicol Lett* 20:33–39.

Yao H, Zhou K, Yan D, Li M, and Wang Y (2009) The Kv2.1 channels mediate neuronal apoptosis induced by excitotoxicity. *J Neurochem* 108:909–919.

Yeh CY, Bulas AM, Moutal A, Saloman JL, Hartnett KA, Anderson CT, Tzounopoulos T, Sun D, Khanna R, and Aizenman E (2017) Targeting a potassium channel/syntaxin interaction ameliorates cell death in ischemic stroke. *J Neurosci* 37:5648–5658.

Yu SP (2003) Regulation and critical role of potassium homeostasis in apoptosis. *Prog Neurobiol* 70:363–386.

Yu SP, Canzoniero LM, and Choi DW (2001) Ion homeostasis and apoptosis. *Curr Opin Cell Biol* 13:405–411.

Zhang Y, Wang H, Li J, Jimenez DA, Levitan ES, Aizenman E, and Rosenberg PA (2004) Peroxynitrite-induced neuronal apoptosis is mediated by intracellular zinc release and 12-lipoxygenase activation. *J Neurosci* 24:10616–10627.

Zhou K, Shi L, Wang Y, Chen S, and Zhang J (2016) Recent advances of the NLRP3 inflammasome in central nervous system disorders. *J Immunol Res* 2016:9238290.

Zhou MH, Yang G, Jiao S, Hu CL, and Mei YA (2012) Cholesterol enhances neuron susceptibility to apoptotic stimuli via cAMP/PKA/CREB-dependent up-regulation of Kv2.1. *J Neurochem* 120:502–514.

Address correspondence to: Dr. Elias Aizenman, Department of Neurobiology, University of Pittsburgh School of Medicine, Pittsburgh, PA 15261. E-mail: redox@pitt.edu